Supporting information

Development of G-quadruplex ligand for selective induction of parallel type topology

Yue Ma,[a] Yamato Tsushima,[a] Mai Sakuma,[a] Shogo Sasaki,[a] Keisuke Iida,[b] Sachiko Okabe,[c] Hiroyuki Seimiya,[c] Takatsugu Hirokawa,[d,e,f] Kazuo Nagasawa*[a]

[a] Department of Biotechnology and Life Science, Tokyo University of Agriculture and Technology, 2-24-16 Naka-cho, Koganei, Tokyo 184-8588 (Japan)
E-mail: knaga@cc.tuat.ac.jp

[b] Department of Chemistry, Chiba University, 1-33 Yayoi, Inage, Chiba 263-8522 (Japan)

[c] Division of Molecular Biotherapy, Cancer Chemotherapy Center, Japanese Foundation for Cancer Research, 3-8-1 Ariake, Koto-ward, Tokyo 135-8550 (Japan)

[d] Transborder Medical Research center, University of Tsukuba, 1-1-1 Tennodai, Tsukuba, 305-8575 (Japan)

[e] Division of Biomedical Science, University of Tsukuba, 1-1-1 Tennodai, Tsukuba, 305-8575 (Japan)

[f] Molecular Profiling Research Center for Drug Discovery, National Institute of Advanced Industrial Science and Technology, 2-4-7 Aomi, Koto-ward, Tokyo 135-0064 (Japan)

Table of Contents:

1. Supplementary Methods

PCR stop assay

The PCR stop assay was performed by means of a modified protocol of the previous study.[1] Sequences of the test oligonucleotides, including telo24 and telo24 mut, and the corresponding complementary sequence (telo24 rev) used in the current study were presented in Table S1. The chain extension reaction was performed in a final volume of 25 μL, in 1 x PCR buffer, containing 0.1 mM dNTP, 1.5 U *Taq* polymerase, 50 pmol of each oligonucleotides and various concentrations of G4 ligands (**1**, **3**, and **4**). The mixture was incubated in a thermocycler with following cycling conditions: 94 ˚C for 2 min, followed by 30 cycles of 94 ˚C for 30 sec, 58 ˚C for 1 min. Amplified PCR products were resolved on 12 % native polyacrylamide gels in 1 X TBE buffer and stained with SYBR Green. Fluorescence was scanned with a phosphorimager (Typhoon 8600, Molecular Dynamics).

CD melting analysis

A solution of 10 μM oligonucleotide (telo24) was performed in 50 mM Tri-HCl buffer without ion. Subsequently, 50 μM ligands (**1**, **3**, and **4**) were added. Melting curves were obtained by monitoring the CD intensity at 265 or 290 nm on a J-720 spectropolarimeter (JASCO, Tokyo, JAPAN) by using a quartz cell of 1 mm optical path length, and the temperature was stepwise increase of 5 ˚C from 25 to 100 ˚C.

2. Supplementary Reference

[1] T. Lemarteleur, D. Gomez, R. Paterski, E. Mandine, P. Mailliet and J. F. Riou, *Biochem. Biophys. Res. Commun.* **2004**, *323*, 802.

3. Oligonucleotides Sequences

Table S1. Sequences of oligonucleotides used in this paper

Oligonucleotide	Sequence
Flu-telo21	5'-FAM-d[GGG TTA GGG TTA GGG TTAGGG]-TAMRA-3'
Flu-dsDNA	5'-FAM-d[TAT AGC TAT ATT TTT TTA TAG CTA TA]-TAMRA-3'
telo24	5'-d[TTA GGG TTA GGG TTA GGGTTA GGG]- 3'
telo24 mut	5'-d[TTA CCC TTA CCC TTA CCC TTA GGG]- 3'
telo rev	5'-d[TCT CGT CTT CCC TAA]- 3'
bcl-2	5'-d[GGG CGC GGG AGG AAT TGG GCG GG]- 3'
TBA	5'-d[GGT TGG TGT GGT TGG]- 3'
Bio-telo24	5'-Biotin-d[TTA GGG TTA GGG TTA GGG TTA GGG]- 3'

4. Circular dichroism (CD) spectrometry

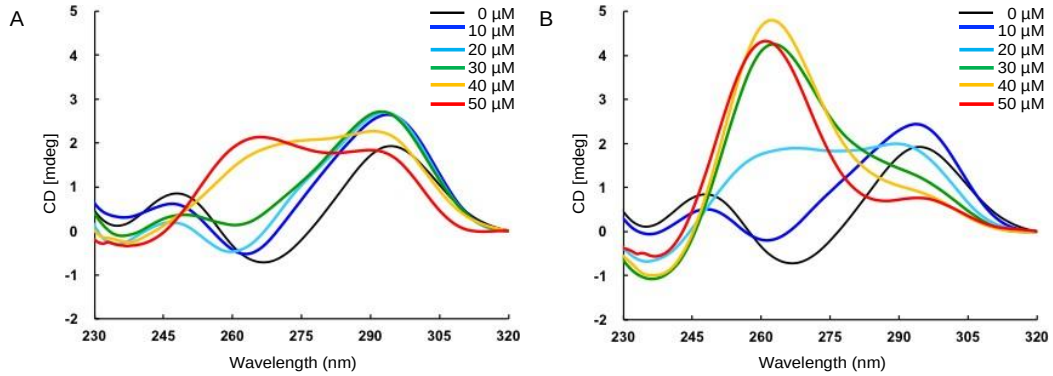

Figure S1. CD spectra of telo24 (10 µM) in 50 mM Tris-HCl buffer (with 50 mM NaCl, pH 7.5) in the presence of 0-5 equivalents of ligand; A) L2H2-2M2EA-6OTD (**3**); B) L2G2-2M2EG-6OTD (**4**).

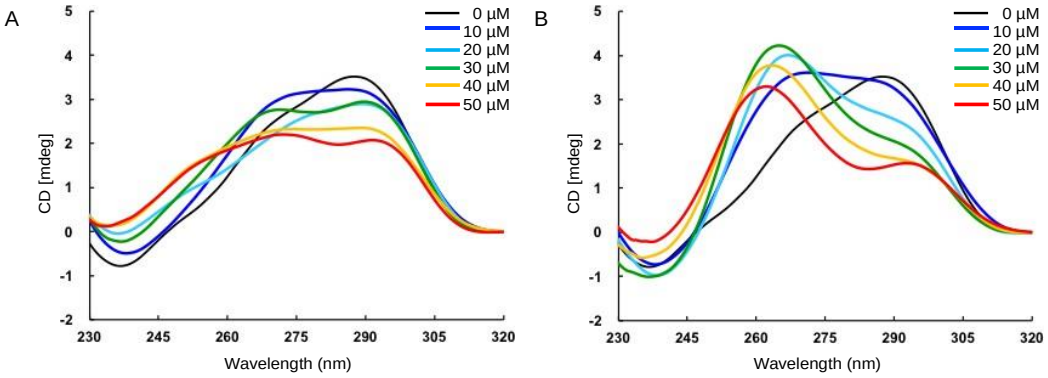

Figure S2. CD spectra of telo24 (10 µM) in 50 mM Tris-HCl buffer (with 50 mM KCl, pH 7.5) in the presence of 0-5 equivalents of ligand; A) L2H2-2M2EA-6OTD (**3**); B) L2G2-2M2EG-6OTD (**4**).

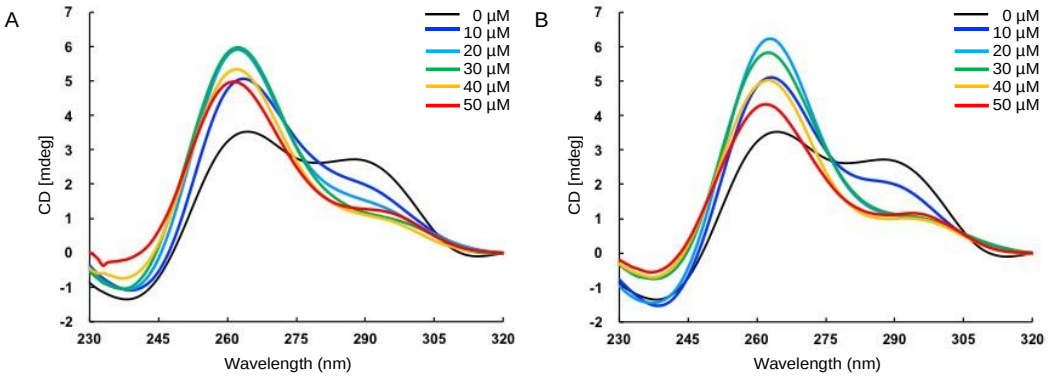

Figure S3. CD spectra of *bcl-2* (10 µM) in 50 mM Tris-HCl buffer (with 50 mM KCl, pH 7.5) in the presence of 0-5 equivalents of ligand; A) L2H2-2M2EA-6OTD (**3**); B) L2G2-2M2EG-6OTD (**4**).

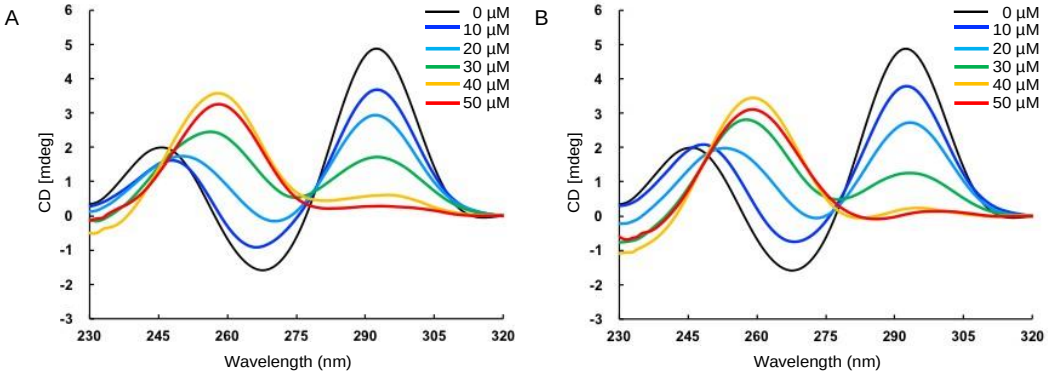

Figure S4. CD spectra of TBA (10 µM) in 50 mM Tris-HCl buffer (with 50 mM KCl, pH 7.5) in the presence of 0-5 equivalents of ligand; A) L2H2-2M2EA-6OTD (**3**); B) L2G2-2M2EG-6OTD (**4**).

5. Surface Plasmon Resonance (SPR) assay

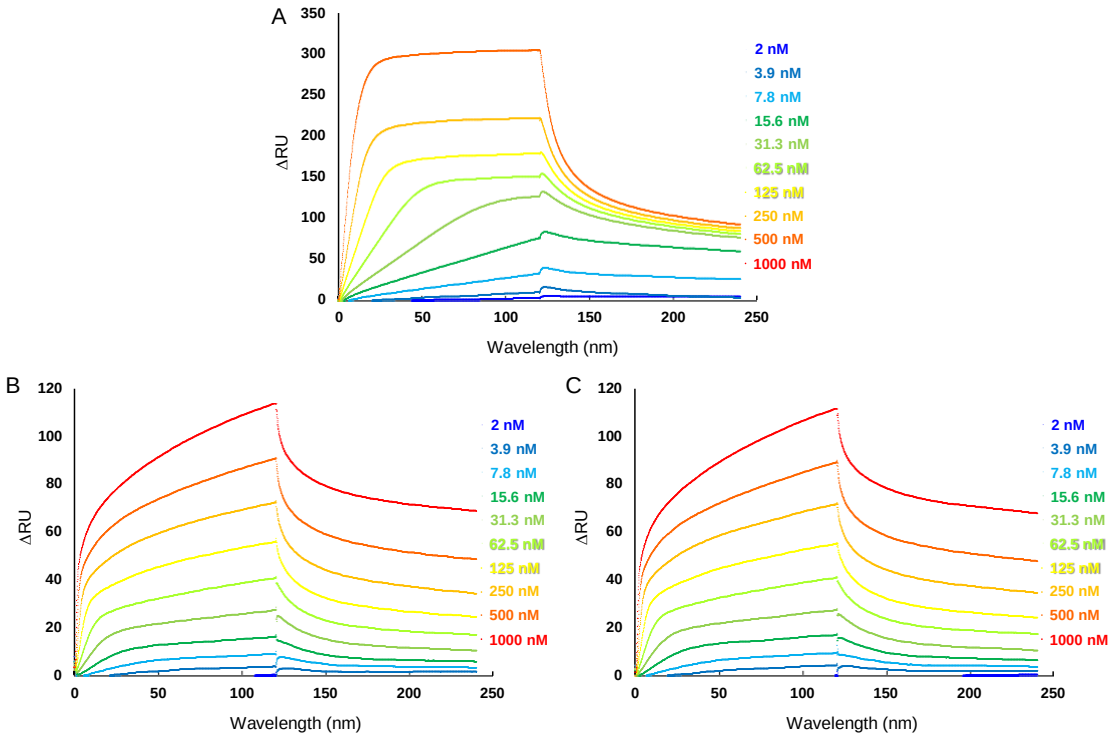

Figure S5. SPR profile of Bio-telo24 bound to ligands; A) L2H2-6OTD (**1**); B) L2H2-2M2EA-6OTD (**3**); C) L2G2-2M2EG-6OTD (**4**).

Table S2. Kinetic parameters for G-quadruplex of Bio-telo24

Ligands	k_a (M^{-1} s^{-1})	k_d (s^{-1})	K_D (nM)
L2H2-6OTD (**1**)	1.5 x 10^6	4.8 x 10^{-2}	31
L2G2-6OTD-2M2EG (**4**)	4.1 x 10^4	3.0 x 10^{-3}	74

6. PCR stop assay

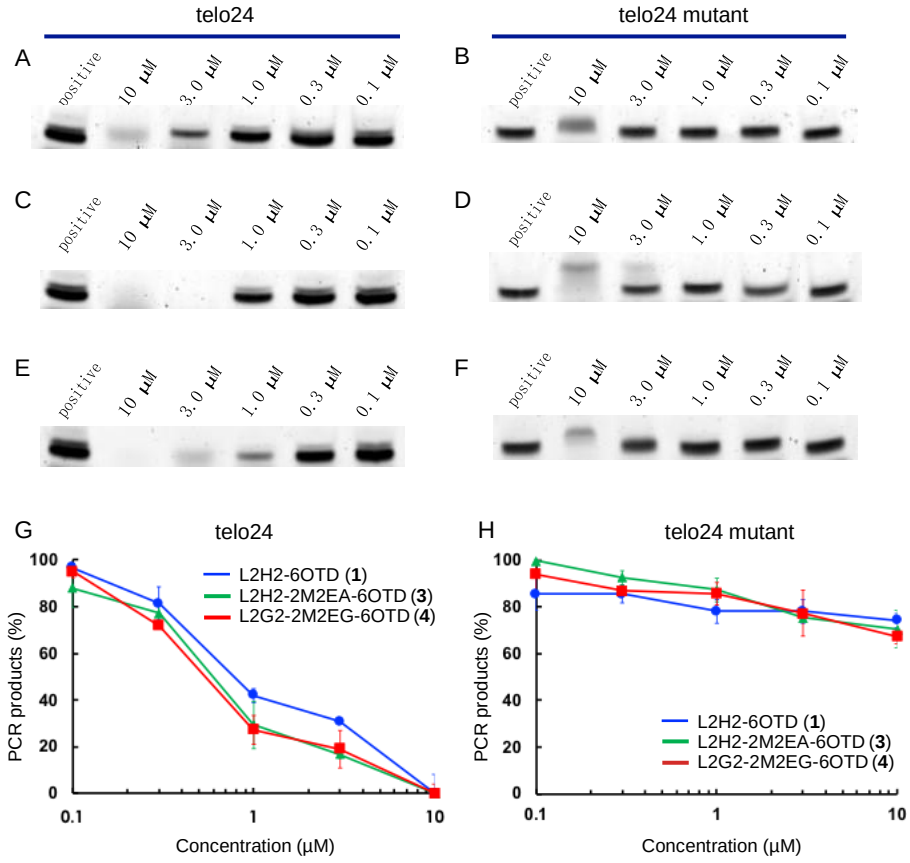

Figure S6. PCR stop assay of **1**, **3**, and **4**. A-F presented the PCR products; A) telo24-**1**; B) telo24 mut-**1**; C) telo24-**3**; D) telo24 mut-**3**; E) telo24-**4**; F) telo24 mut-**4**. G and H presented the quantification of the fluorescent intensity by using phosphorimager; G) telo24-(**1**, **3** and **4**); H) telo24 mut-(**1**, **3** and **4**).

Table S3. DNA sequence selectivity of 6OTDs **1**, **3**, and **4** by the PCR stop assay

Ligands	telo24	telo24 mut
	IC_{50} (μM)	
L2H2-6OTD (**1**)	0.86 ± 0.1	>10
L2H2-6OTD-2M2EA (**3**)	0.70 ± 0.04	>10
L2G2-6OTD-2M2EG (**4**)	0.65 ± 0.01	>10

7. CD melting analysis

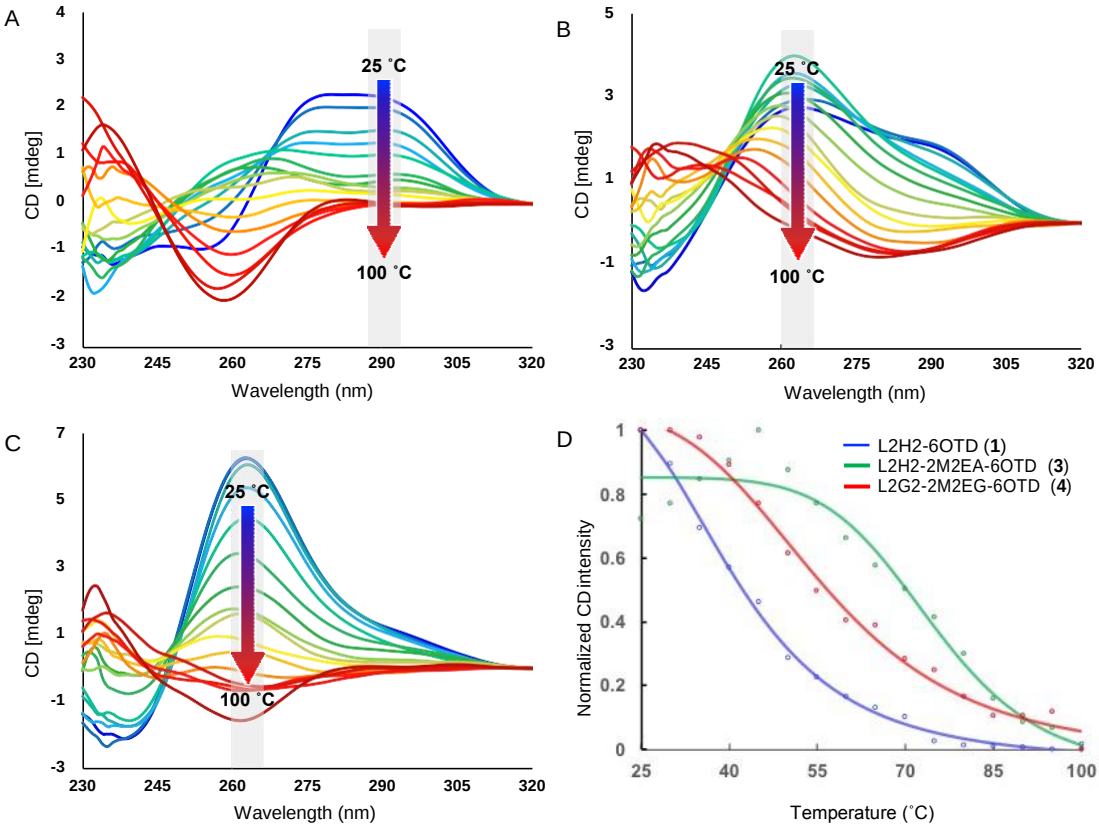

Figure S7. CD melting assay of **1**, **3**, and **4** with telo24. The CD melting profiles for telo24 with ligands; A) L2H2-6OTD (**1**); B) L2H2-2M2EA-6OTD (**3**); C) L2G2-2M2EG-6OTD (**4**). D) The CD melting curves of telo24 were recorded at 290 nm in the presence of **1**, and at 265 nm in the presence of **3** and **4**, respectively.

8. TRAP assay

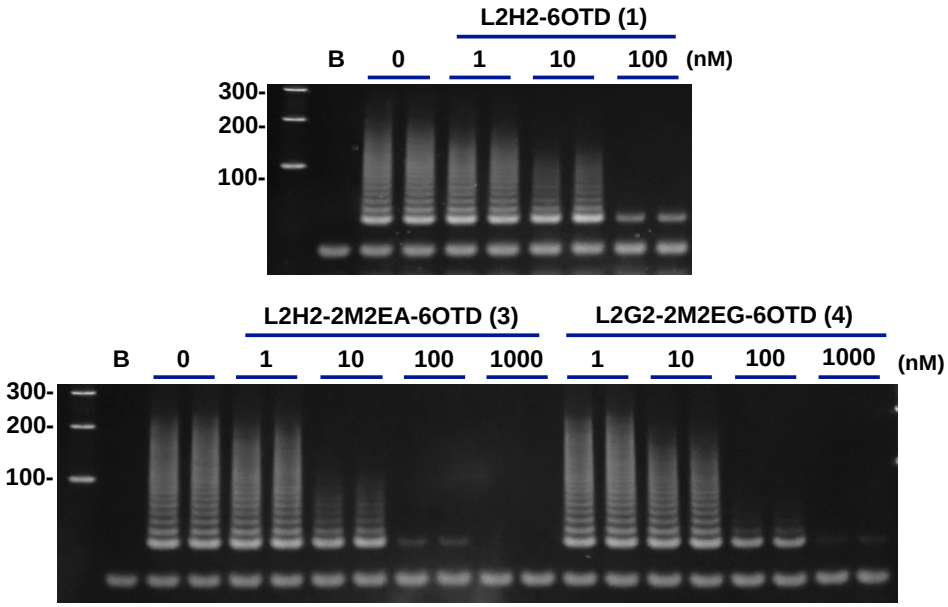

Figure S8. TRAP assay for ligand **1**, **3**, and **4**.

Table S4. Telomerase inhibitory activities of 6OTDs **1**, **3**, and **4** by the TRAP assay

Ligands	IC_{50} (nM)
L2H2-6OTD (**1**)	97.5
L2H2-6OTD-2M2EA (**3**)	6.8
L2G2-6OTD-2M2EG (**4**)	40.3

9. Magnified view of docking model (Figure 2)

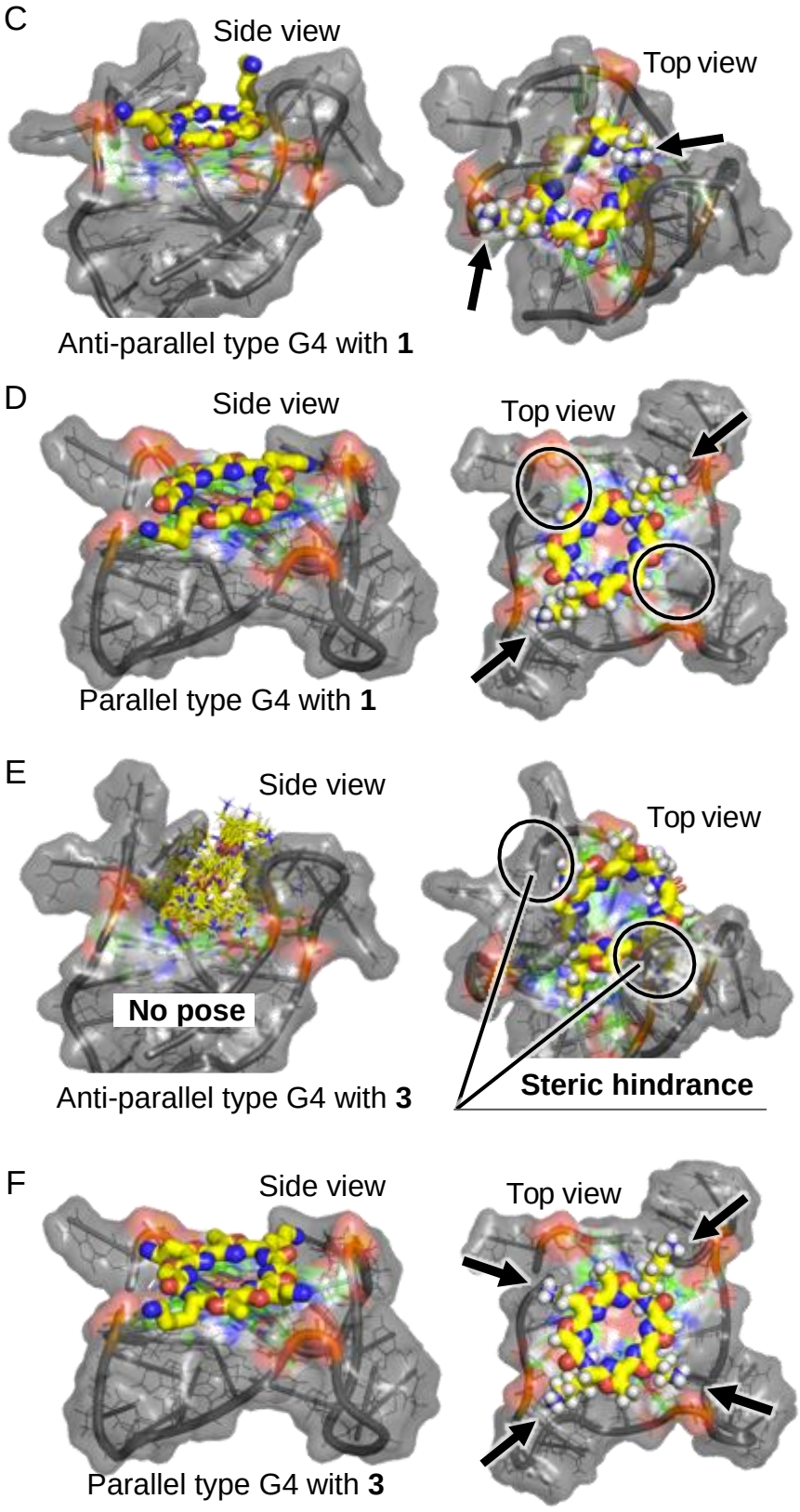

10. ^{1}H and ^{13}C NMR spectra for 8, 9, 3, 10, 4.

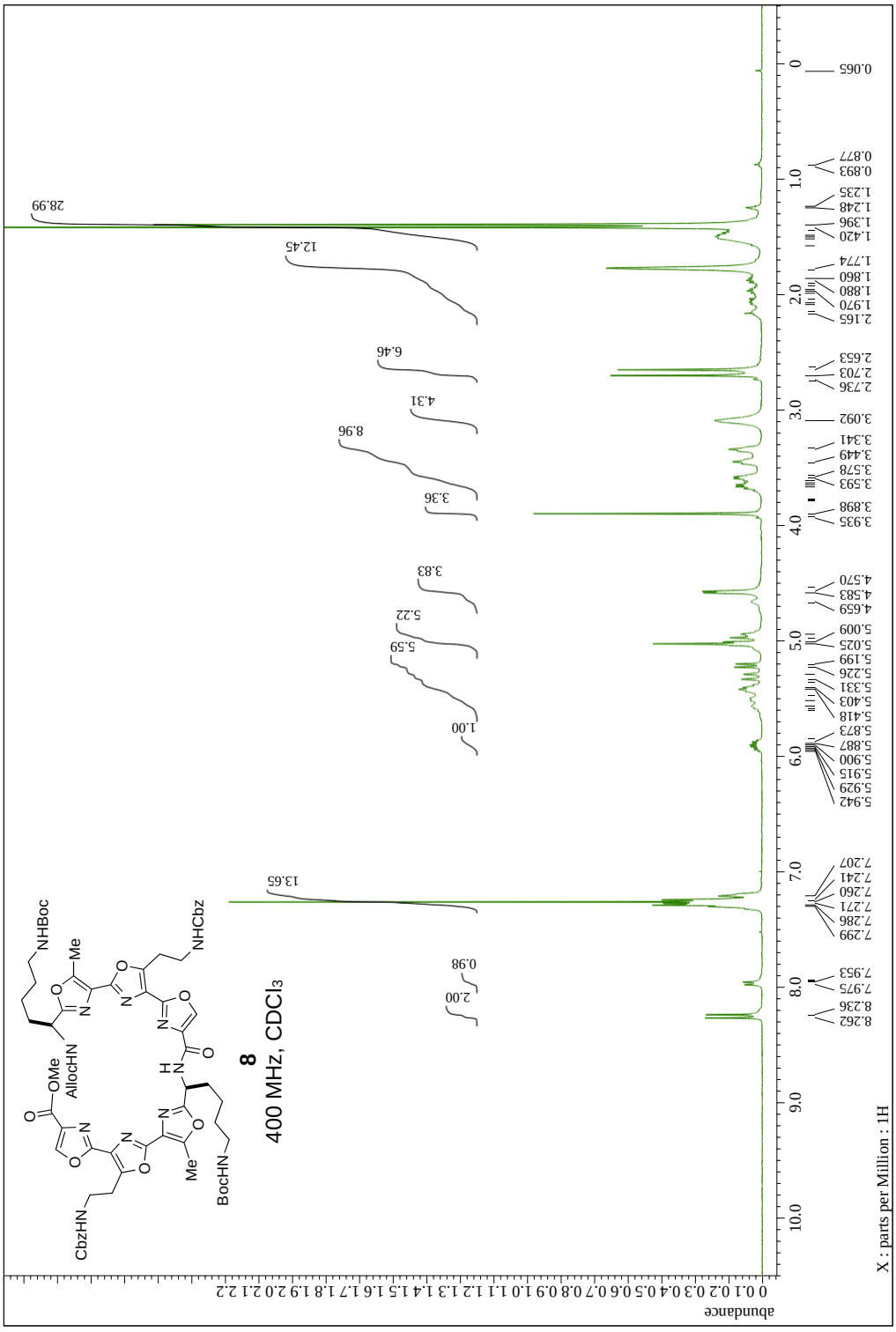

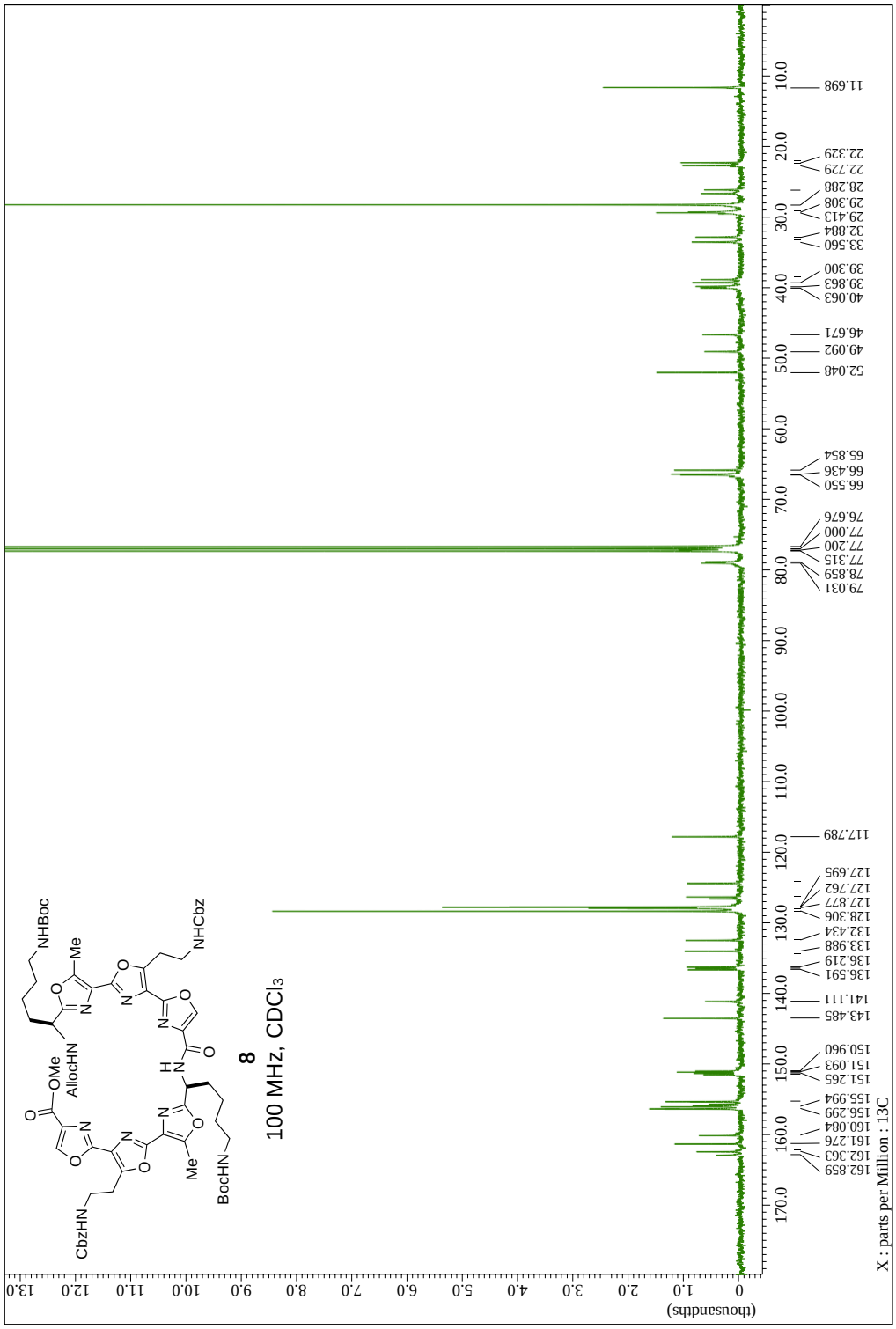
8
100 MHz, CDCl3
X : parts per Million : 13C
(thousandths)
11.698
22.329
22.729
28.288
29.308
29.413
32.884
33.560
39.300
39.863
40.063
46.671
49.092
52.048
65.854
66.436
66.550
76.676
77.000
77.200
77.315
78.859
79.031
117.789
127.695
127.762
127.877
128.306
132.434
133.988
136.219
136.591
141.111
143.485
150.960
151.093
151.265
155.994
156.299
160.084
161.276
162.363
162.859

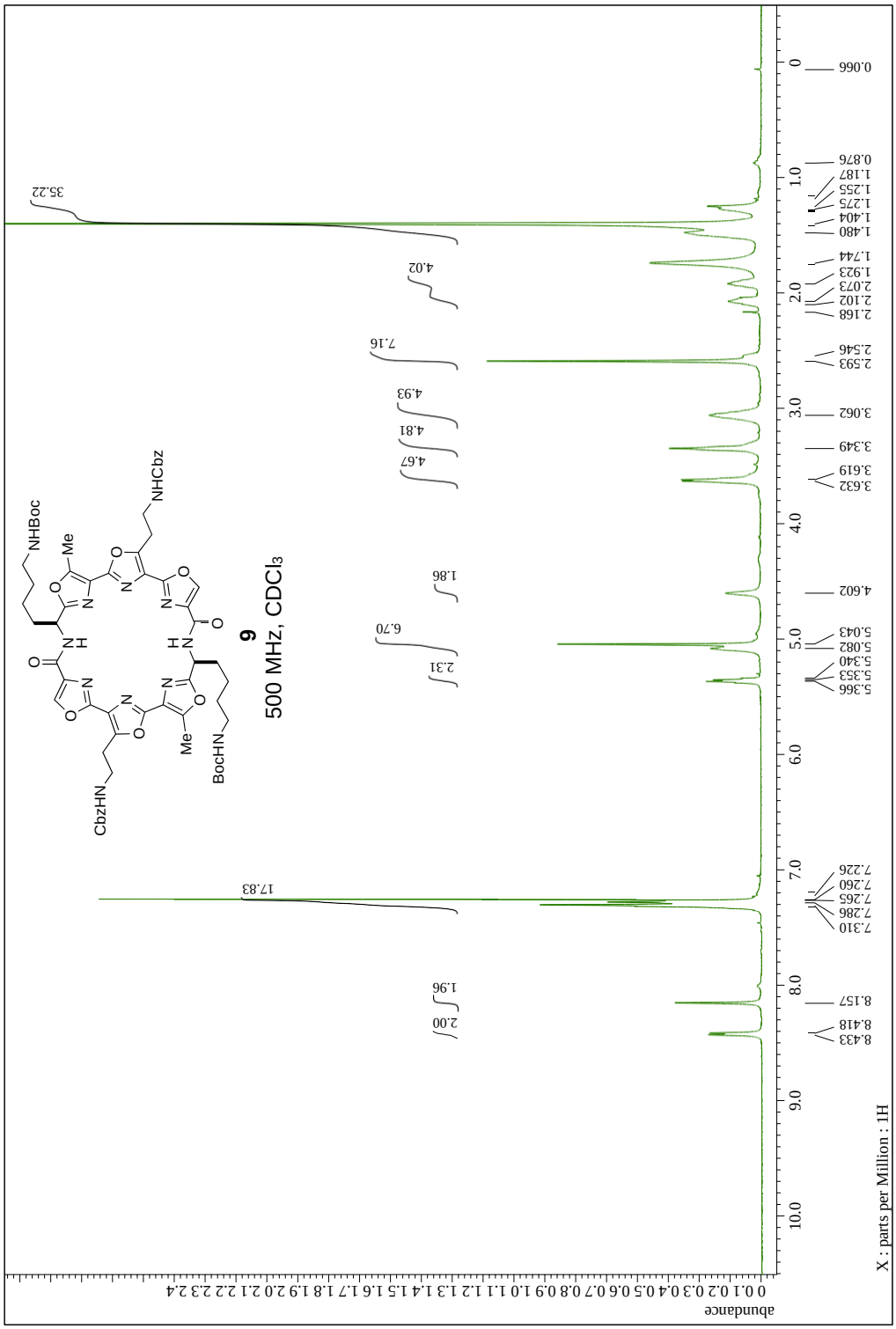
9
500 MHz, CDCl3
NHBoc
Me
NHCbz
CbzHN
BocHN
Me
35.22
17.83
7.16
6.70
4.93
4.81
4.67
4.02
2.31
2.00
1.96
1.86
X : parts per Million : 1H
abundance

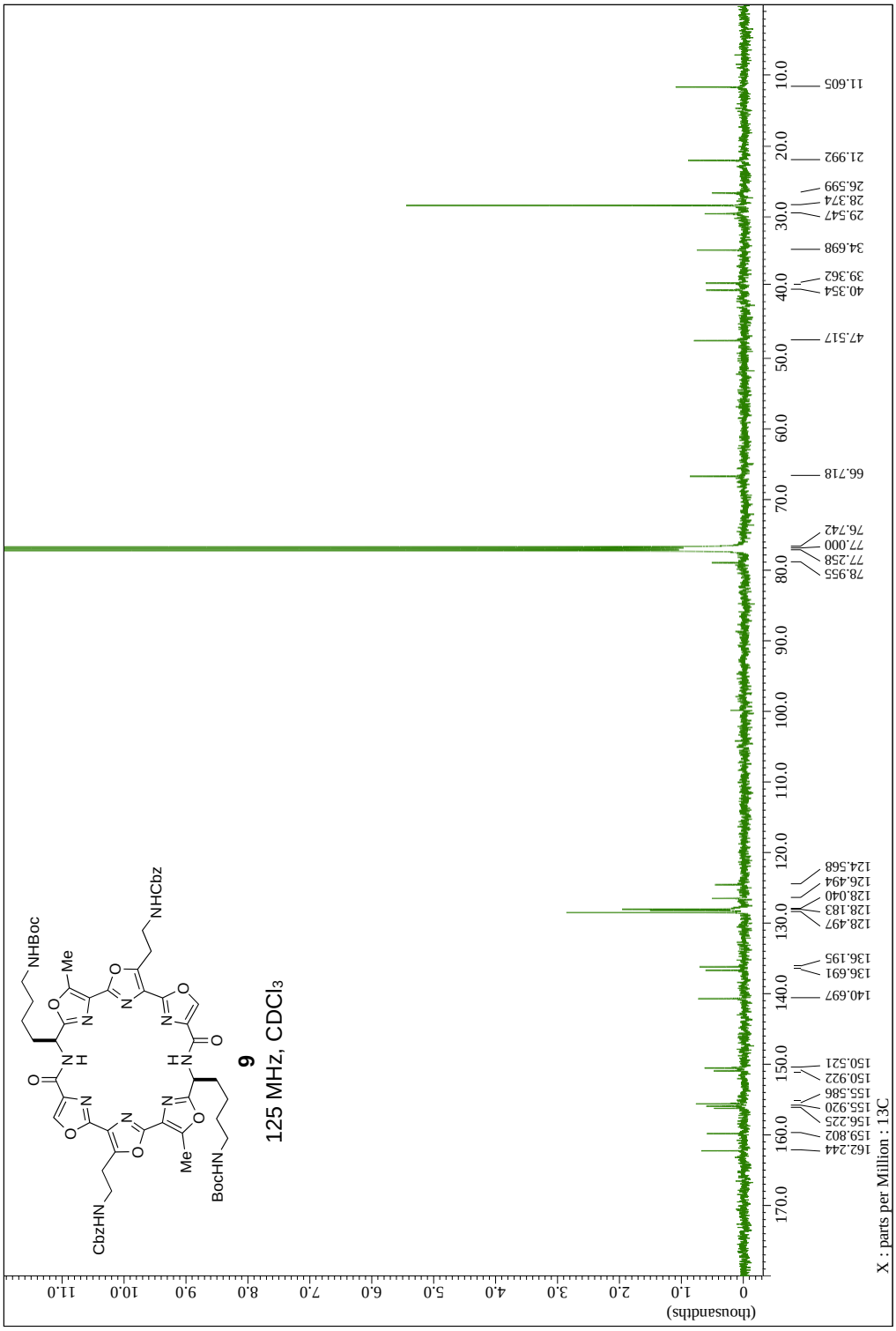
9
125 MHz, CDCl3
NHBoc
Me
NHCbz
CbzHN
BocHN
Me
(thousandths)
X : parts per Million : 13C
11.605
21.992
26.599
28.374
29.547
34.698
39.362
40.354
47.517
66.718
76.742
77.000
77.258
78.955
124.568
126.494
128.040
128.183
128.497
136.195
136.691
140.697
150.521
150.922
155.586
155.920
156.225
159.802
162.244

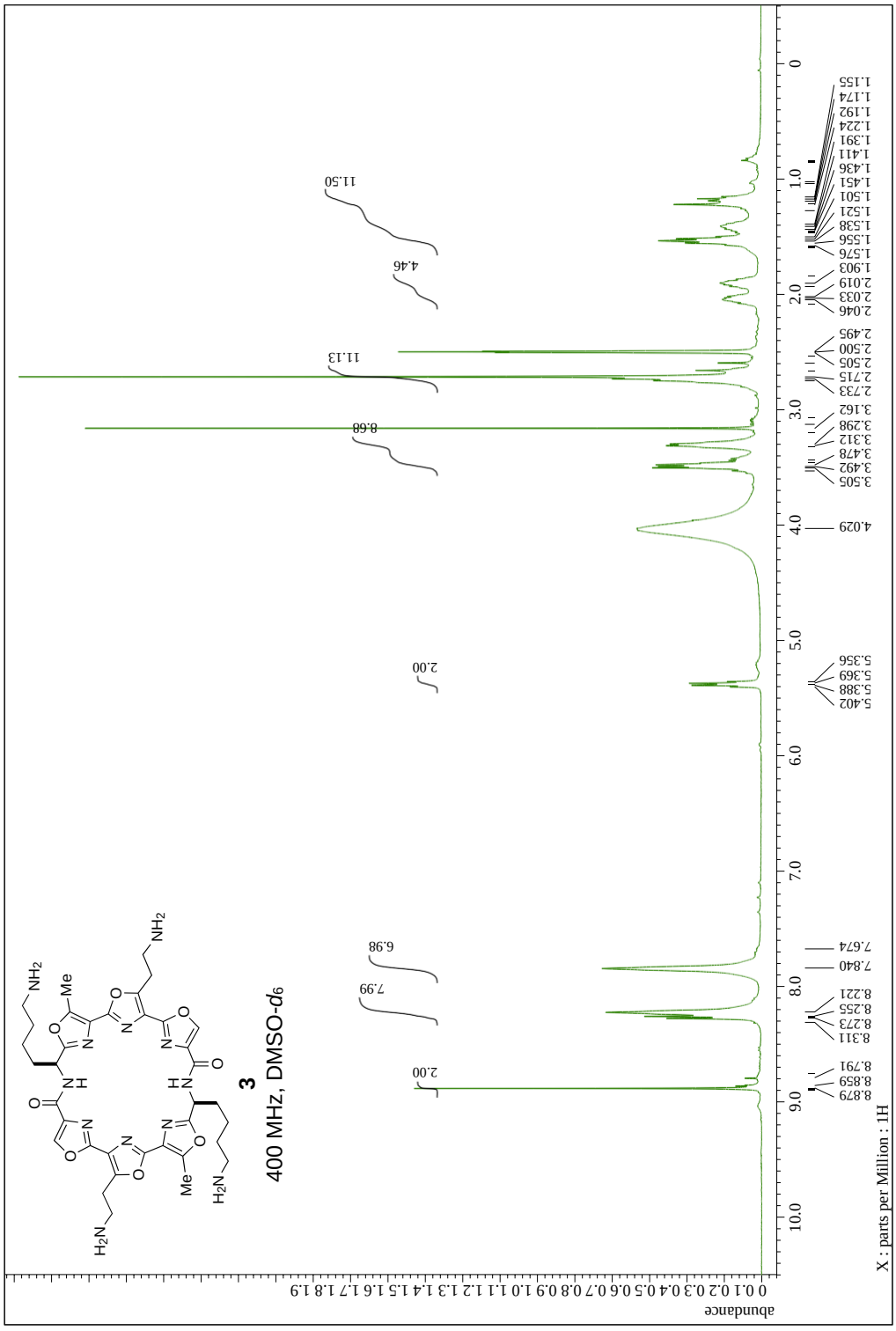
3
400 MHz, DMSO-d6
X : parts per Million : 1H
abundance
11.50
4.46
11.13
8.68
7.99
6.98
2.00
2.00
4.029
8.879
8.859
8.791
8.311
8.273
8.255
8.221
7.840
7.674
5.402
5.388
5.369
5.356
3.505
3.492
3.478
3.312
3.298
3.162
2.733
2.715
2.505
2.500
2.495
2.046
2.033
2.019
1.903
1.576
1.556
1.538
1.521
1.501
1.451
1.436
1.411
1.391
1.224
1.192
1.174
1.155

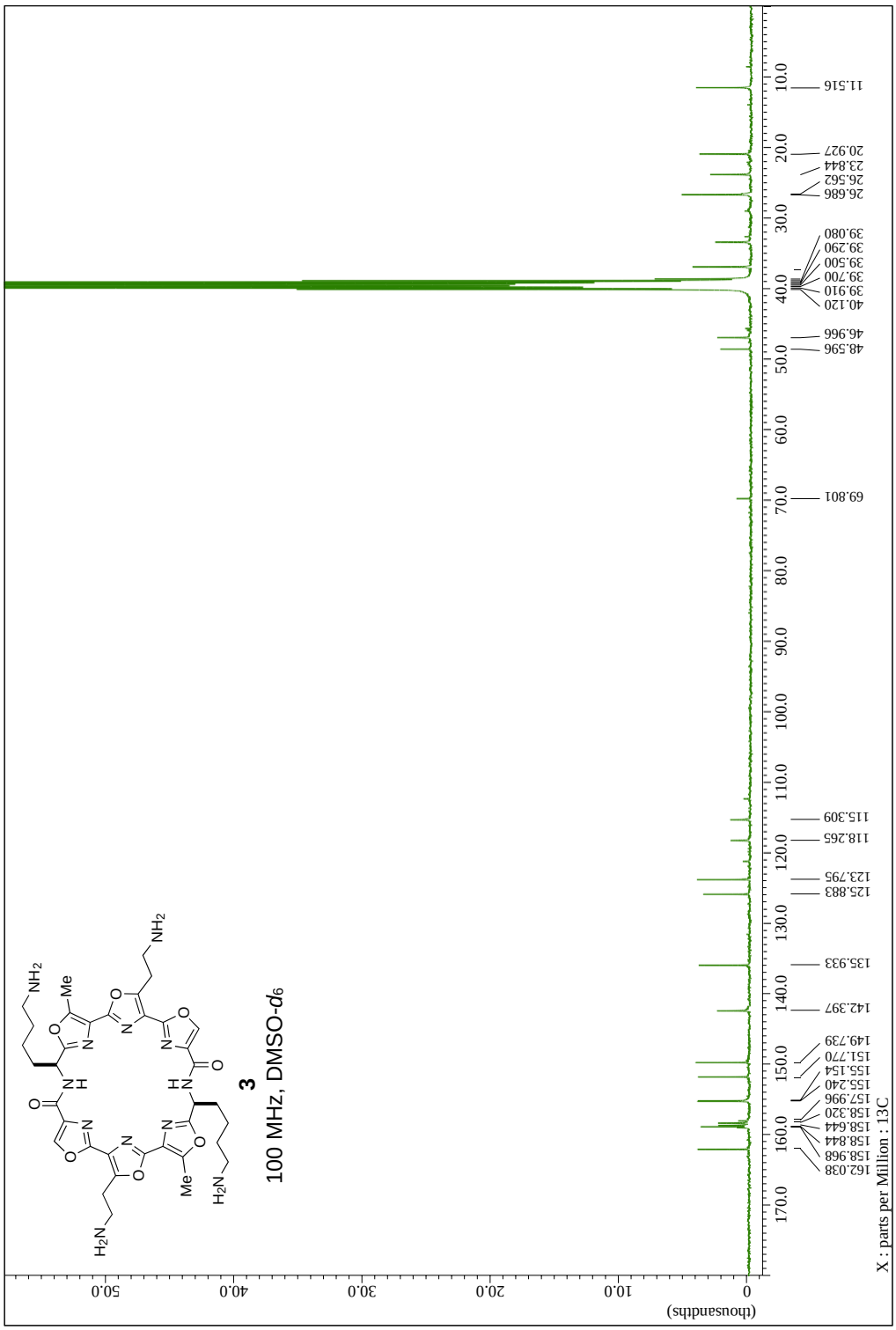
3
100 MHz, DMSO-d_6
X : parts per Million : 13C
(thousandths)
162.038
158.968
158.844
158.644
158.320
157.996
155.240
155.154
151.770
149.739
142.397
135.933
125.883
123.795
118.265
115.309
69.801
48.596
46.966
40.120
39.910
39.700
39.500
39.290
39.080
26.686
26.562
23.844
20.927
11.516

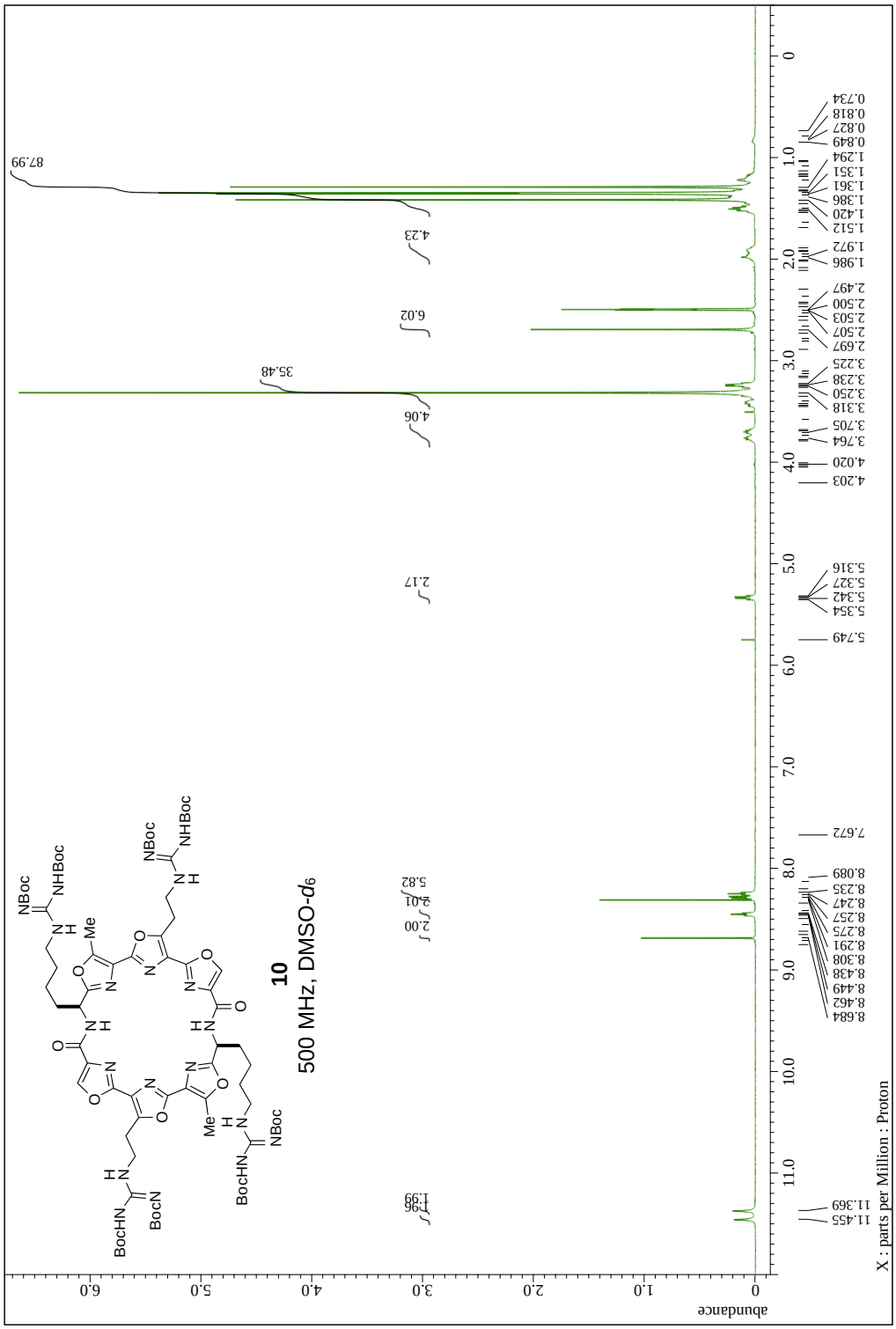
10
500 MHz, DMSO-d6
X : parts per Million : Proton
abundance

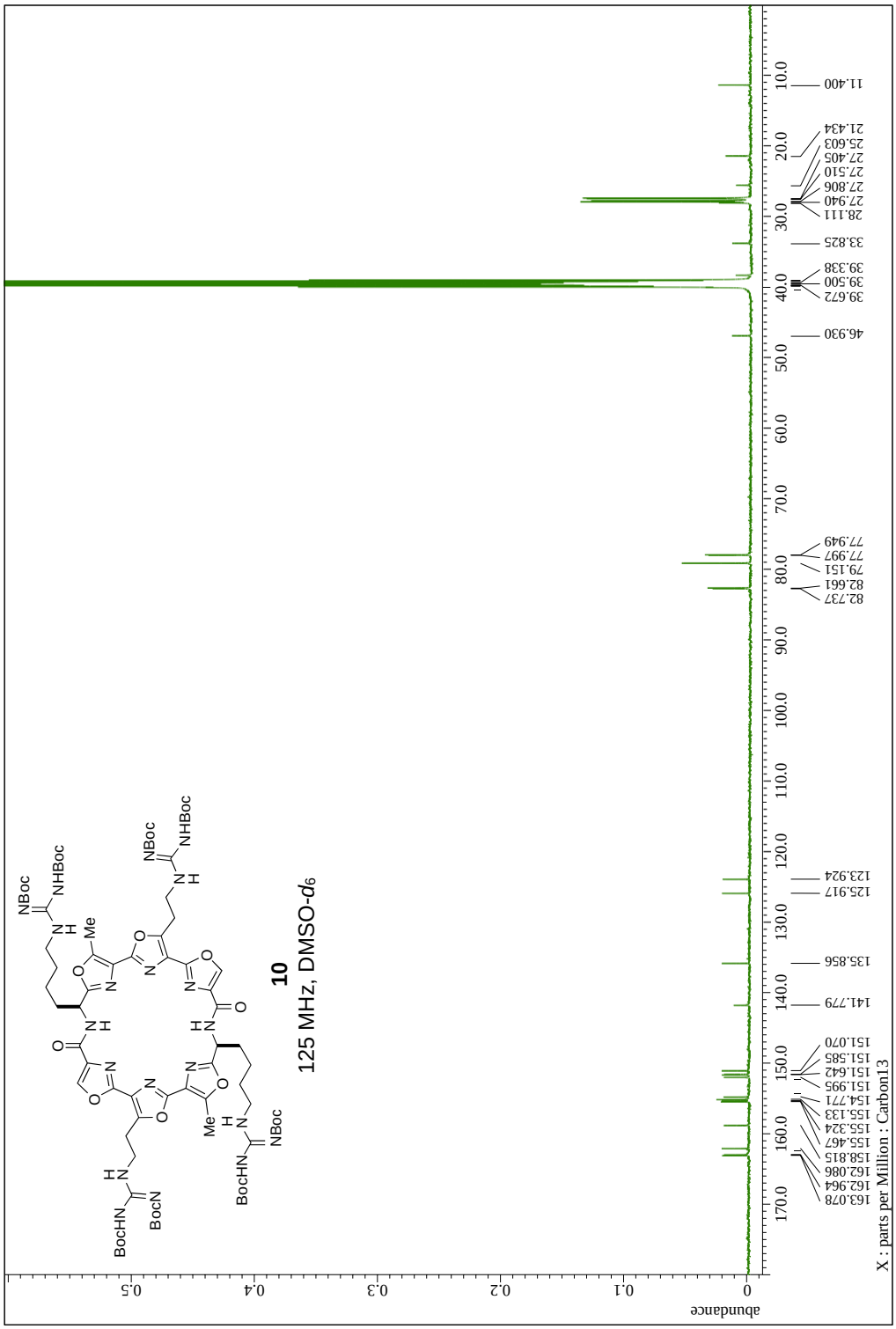
10
125 MHz, DMSO-d_6
X : parts per Million : Carbon13
abundance
11.400
21.434
25.603
27.405
27.510
27.806
27.940
28.111
33.825
39.338
39.500
39.672
46.930
77.949
77.997
79.151
82.661
82.737
123.924
125.917
135.856
141.779
151.070
151.585
151.642
151.995
154.771
155.133
155.324
155.467
158.815
162.086
162.964
163.078

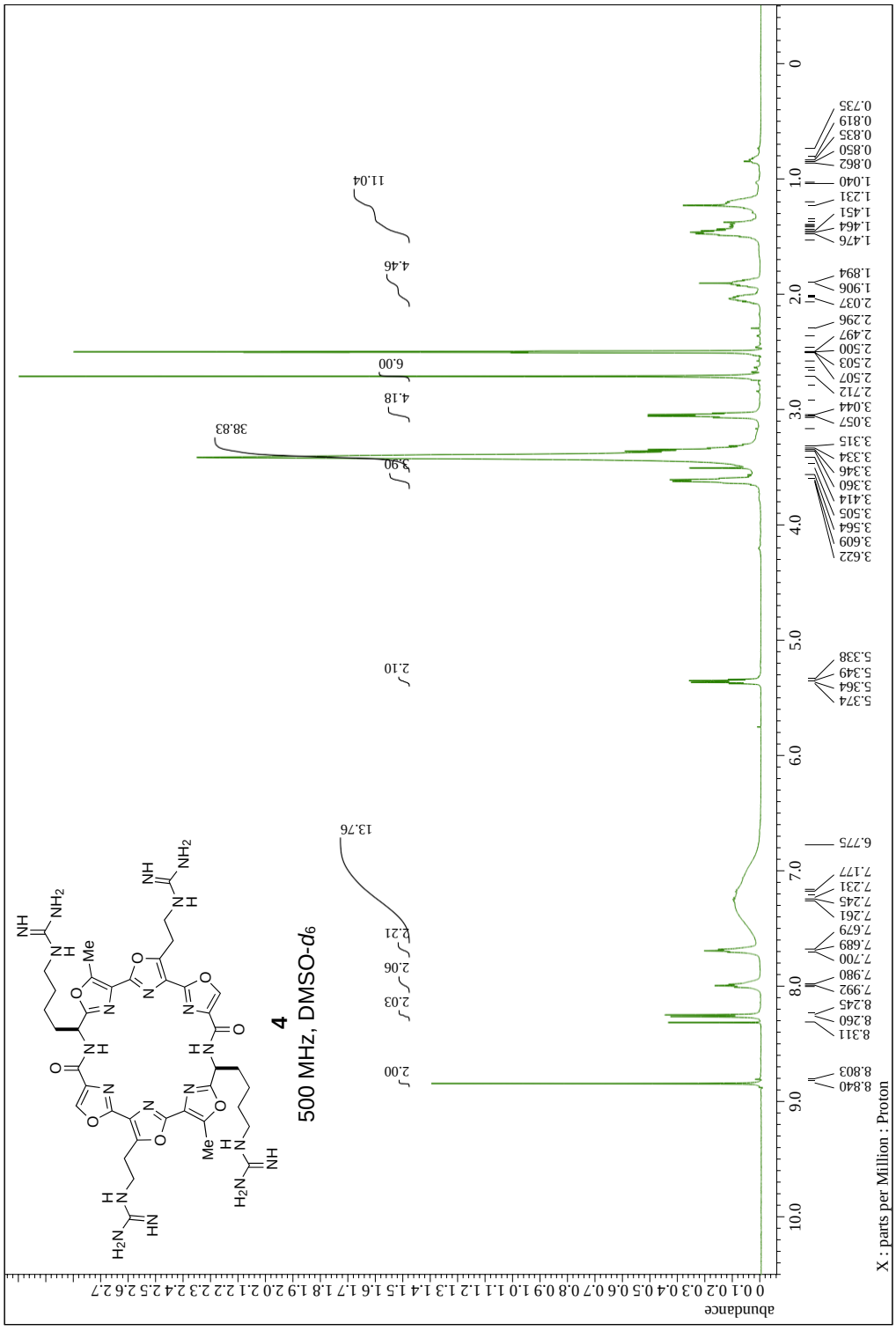
4
500 MHz, DMSO-d6
X : parts per Million : Proton
abundance
13.76
11.04
38.83
6.00
4.46
4.18
3.90
2.21
2.10
2.06
2.03
2.00

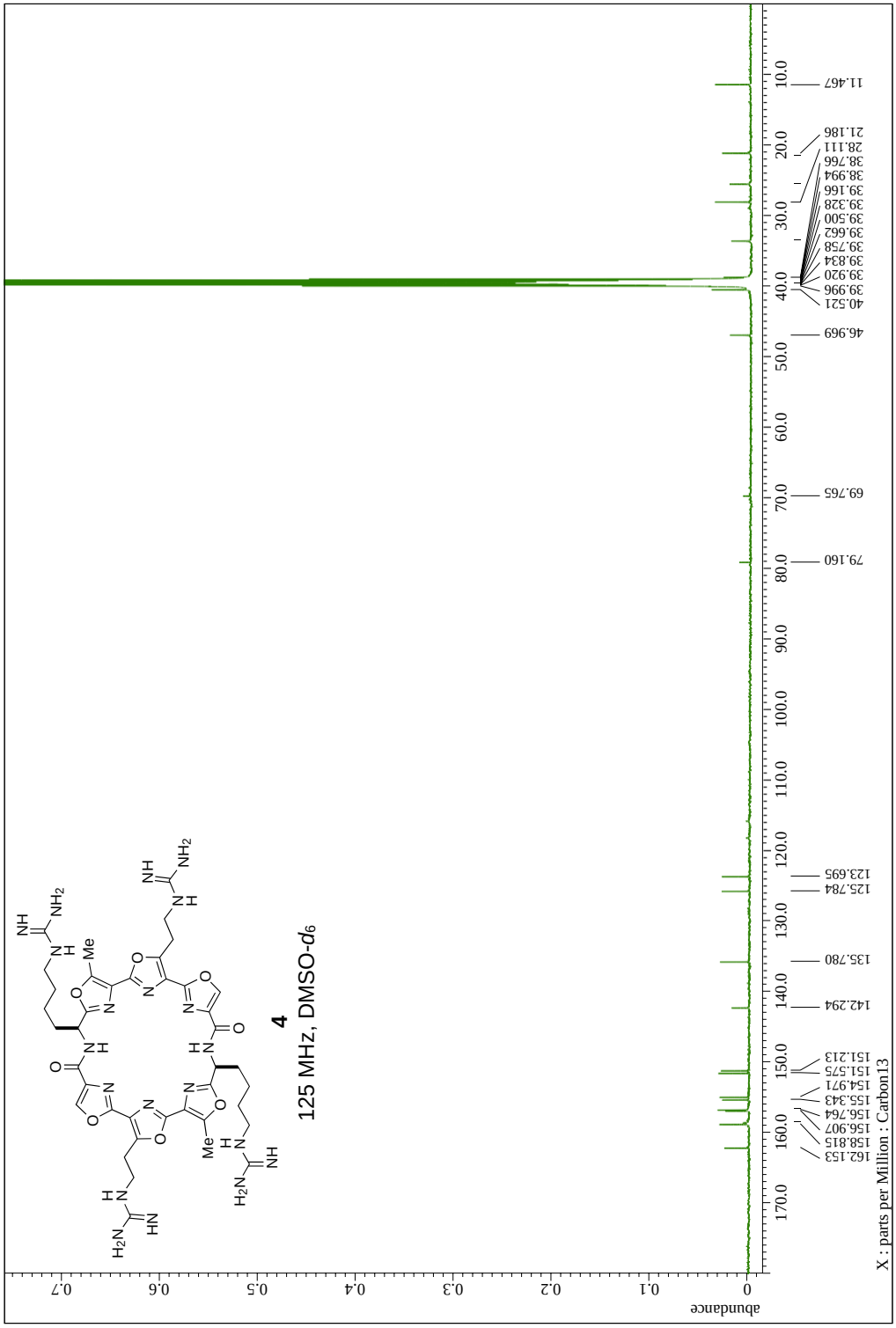
4
125 MHz, DMSO-d_6
abundance
X : parts per Million : Carbon13
11.467
21.186
28.111
38.766
38.994
39.166
39.328
39.500
39.662
39.758
39.834
39.920
39.996
40.521
46.969
69.765
79.160
123.695
125.784
135.780
142.294
151.213
151.575
154.971
155.343
156.764
156.907
158.815
162.153